Electronic and structural properties of low-temperature superconductors and ternary pnictides $A\mathrm{Ni}_2Pn_2$ (A=Sr,Ba and Pn=P,As)

I. R. Shein* and A. L. Ivanovskii

Institute of Solid State Chemistry, Ural Branch of the Russian Academy of Sciences, Ekaterinburg GSP-145 620041, Russia

(Received 14 November 2008; published 11 February 2009)

Based on first-principles full-potential linearized augmented plane wave method (FLAPW)–generalized gradient approximation calculations, we have investigated structural and electronic properties of low-temperature superconductors $\mathrm{SrNi}_2\mathrm{As}_2$ ($T_C \sim 0.6$ K), $\mathrm{BaNi}_2\mathrm{As}_2$ ($T_C \sim 0.7$ K), and $\mathrm{BaNi}_2\mathrm{P}_2$ ($T_C \sim 3$ K), as well as $\mathrm{SrNi}_2\mathrm{P}_2$. Our results show that the replacement of alkaline-earth metal (Sr↔Ba) and pnictogen (P↔As) types leads to *anisotropic deformations* of crystal structure caused by strong anisotropy of interatomic bonds. The band structure, density of states, and Fermi-surface features for $(\mathrm{Sr,Ba})\mathrm{Ni}_2(\mathrm{P,As})_2$ are evaluated and discussed. As distinct from $(\mathrm{Ca,Sr,Ba})\mathrm{Fe}_2\mathrm{As}_2$—the parent phases for "122" FeAs superconductors—the Fermi level in $(\mathrm{Sr,Ba})\mathrm{Ni}_2(\mathrm{P,As})_2$ phases is shifted to the bands with higher dispersion $E(k)$ but lower density of states as a result of increased electron concentration. Therefore the Fermi surfaces for $(\mathrm{Sr,Ba})\mathrm{Ni}_2(\mathrm{P,As})_2$ phases differ essentially from those of the FeAs-based materials and adopt a multisheet three-dimensional type. Our estimations show that $(\mathrm{Sr,Ba})\mathrm{Ni}_2(\mathrm{P,As})_2$ are within the weak-coupling limit with a small average electron-phonon coupling constant $\lambda_{ep} \sim 0.16-0.24$. The bonding in $(\mathrm{Sr,Ba})\mathrm{Ni}_2(\mathrm{P,As})_2$ is of a complex anisotropic character. Namely, the bonding in [NiP(As)] layers may be described as a mixture of metallic, ionic, and covalent contributions. In turn, between adjacent [NiP(As)] layers and (Sr,Ba) atomic sheets, ionic bonds emerge, whereas between adjacent [NiP(As)]/[NiP(As)] layers covalent bonds occur owing to hybridization of p states of pnictogen atoms.

DOI: 10.1103/PhysRevB.79.054510 PACS number(s): 71.18.+y, 71.15.Mb, 74.25.Jb

I. INTRODUCTION

The recent discovery[1–7] of copper-free high-temperature superconductors (SCs; with transition temperatures up to $T_C \sim 56$ K) based on quaternary oxyarsenides (the so-called 1111-phase LnFeAsO, where Ln are early rare-earth metals such as La, Ce, Sm, Dy, and Gd) aroused tremendous interest in layered FeAs systems and stimulated much activity in the search for new related superconducting materials. Very recently, the family of these FeAs SCs has been extended to oxygen-free ternary arsenides—the so-called 122-phase $A\mathrm{Fe}_2\mathrm{As}_2$ (where A are alkaline-earth metals Ca, Sr, and Ba).[8–13]

Both families of the FeAs SCs have a quasi-two-dimensional (2D) tetragonal crystal structure, in which [FeAs] layers are separated by either [LnO] layers or A atomic sheets. Fe ions form a square lattice sandwiched between two As sheets shifted so that each Fe is surrounded by a distorted As tetrahedron. The most remarkable features of these 1111 and 122 FeAs SCs with an unconventional mechanism of superconductivity are as follows: (i) the nondoped parent compounds LnFeAsO and $A\mathrm{Fe}_2\mathrm{As}_2$ are located on the border of magnetic instability and commonly exhibit temperature-dependent structural and magnetic phase transitions with the formation of collinear antiferromagnetic spin ordering; and (ii) superconductivity emerges by either the hole or electron doping into the parent compounds. Furthermore, the electronic bands in the window around the Fermi level are formed mainly by the states of the [FeAs] layers and play an important role in superconductivity, whereas the [LnO] layers (A atomic sheets) serve as "charge reservoirs."[1–13]

Thus, the atomic substitutions inside the [FeAs] layers should exert the most profound influence on the properties of these 1111 and 122 phases and, in particular, on their superconductivity. For this reason, to gain further insight into the nature of these systems, experimental and theoretical studies focusing on the related layered materials (where [FeAs] layers are replaced, for example, by [FeP], [NiAs], or [NiBi] layers) have been performed.[14–20] In this way among tetragonal ($\mathrm{ThCr}_2\mathrm{Si}_2$ structure type) 122 phases, low-temperature superconductivity has been recently discovered in stoichiometric undoped $\mathrm{SrNi}_2\mathrm{As}_2$ ($T_C \sim 0.6$ K),[18] $\mathrm{BaNi}_2\mathrm{As}_2$ ($T_C \sim 0.7$ K),[19] and $\mathrm{BaNi}_2\mathrm{P}_2$ ($T_C \sim 3$ K).[20]

In this paper we present a systematic study of the structural and electronic properties of and an intra-atomic bonding picture for low-temperature superconductors $\mathrm{SrNi}_2\mathrm{As}_2$, $\mathrm{BaNi}_2\mathrm{As}_2$, and $\mathrm{BaNi}_2\mathrm{P}_2$, and the related phase $\mathrm{SrNi}_2\mathrm{P}_2$.[21] This choice allows us to compare the above properties of these isostructural phases as a function of the alkaline-earth metal type (Sr versus Ba, i.e., $\mathrm{SrNi}_2\mathrm{P}_2 \leftrightarrow \mathrm{BaNi}_2\mathrm{P}_2$ and $\mathrm{SrNi}_2\mathrm{As}_2 \leftrightarrow \mathrm{BaNi}_2\mathrm{As}_2$) and the pnictogen type (P versus As, i.e., $\mathrm{SrNi}_2\mathrm{P}_2 \leftrightarrow \mathrm{SrNi}_2\mathrm{As}_2$ and $\mathrm{BaNi}_2\mathrm{P}_2 \leftrightarrow \mathrm{BaNi}_2\mathrm{As}_2$).

As a result, the optimized lattice parameters, band structures, densities of states (DOSs), and Fermi surfaces (FSs) are presented and analyzed. These data show that $(\mathrm{Sr,Ba})\mathrm{Ni}_2(\mathrm{P,As})_2$ phases adopt remarkably different electronic properties as compared with $A\mathrm{Fe}_2\mathrm{As}_2$ (the parent phases for high-T_C 122 FeAs SCs) owing to higher valence electron count in Ni ions than in Fe ions. Our estimations show also that the Ni-based pnictides $(\mathrm{Sr,Ba})\mathrm{Ni}_2(\mathrm{P,As})_2$ are within the weak-coupling limit with a very small average electron-phonon coupling constant $\lambda_{ep} \sim 0.16-0.24$. Finally, our analysis allows us to classify the bonding in [NiP(As)] layers as a mixture of metallic, ionic, and covalent contributions. Ionic bonds emerge between adjacent [NiP(As)] layers and (Sr,Ba) atomic sheets owing to $(\mathrm{Sr,Ba}) \rightarrow$[NiP(As)]

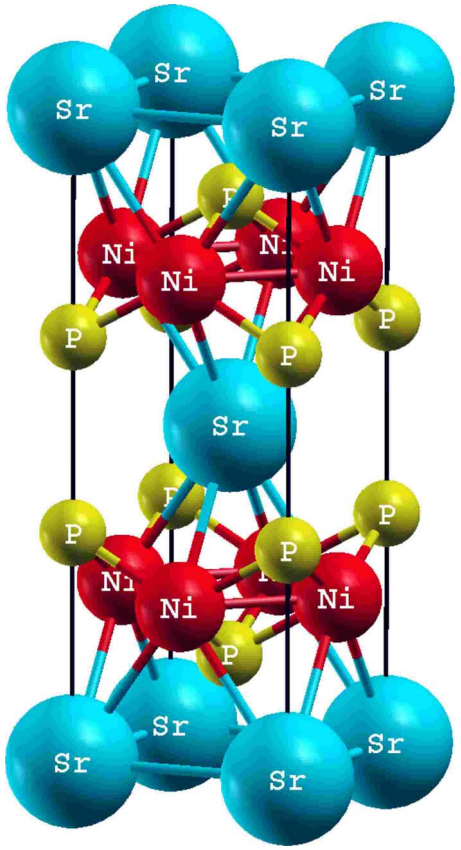

FIG. 1. (Color online) Crystal structure of tetragonal ($ThCr_2Si_2$-like) $SrNi_2P_2$ phase. [NiP] molecular layers and Sr atomic sheets are stacked along the c axis.

charge transfer, whereas covalent bonds arise between the adjacent [NiP(As)]/[NiP(As)] layers as a result of hybridization of the p-p states of pnictogen atoms.

II. COMPUTATIONAL METHOD AND MODELS

The considered ternary arsenides $(Sr,Ba)Ni_2(P,As)_2$ adopt[18–21] a $ThCr_2Si_2$-type tetragonal structure (space group $I4/mmm$; $Z=2$) and are formed by a stack of alternating (Sr,Ba) atomic sheets and [FeP(As)] layers. In turn, these layers are formed by Ni$\{P(As)\}_4$ tetrahedra; see Fig. 1. The atomic positions are for alkaline-earth metals, $2a$ (0,0,0); for Ni, $4d$ $(\frac{1}{2},0,\frac{1}{2})$; and for pnictogen atoms, $4e$ $(0,0,z_{P,As})$, where $z_{P,As}$ are the so-called internal coordinates governing the Ni-(P,As) distances and the distortion of the $\{P(As)\}_4$ tetrahedra around the Ni in the [FeP(As)] layers.

Our band-structure calculations were carried out by means of the full-potential method with mixed basis augmented plane wave (APW)+lo [linearized augmented plane wave (LAPW)] implemented in the WIEN2K suite of programs.[22] The generalized gradient approximation (GGA) correction to exchange-correlation potential in the Perdew-Burke-Ernzerhof (PBE) form[23] was used. The plane-wave expansion was taken to $R_{MT}\times K_{max}$ equal to 7, and the k sampling with $10\times10\times10$ k points in the Brillouin zone was used. The calculations were performed with full-lattice optimization including internal $z_{P,As}$ coordinates. The self-consistent calculations were considered to be converged when the difference in the total energy of the crystal did not exceed 0.1 mRy and the difference in the total electronic charge did not exceed $0.001e$ as calculated at consecutive steps.

TABLE I. The optimized lattice parameters (a and c, in Å), internal coordinates ($z_{P,As}$), some interatomic distances [d(Ni-P(As)), in Å], and angles [(Ni-PAs)-Ni) in deg] for ternary pnictides $SrNi_2P_2$, $SrNi_2As_2$, $BaNi_2P_2$, and $BaNi_2As_2$. Available experimental data are given in parentheses.

Phase/parameter	$SrNi_2P_2$	$SrNi_2As_2$	$BaNi_2P_2$	$BaNi_2As_2$
a	3.947	4.166	3.956	4.148
	(3.948[a])	(4.137[b])	(3.947[a])	(4.112[c])
c	11.069	10.502	11.995	11.901
	(10.677[a])	(10.188[b])	(11.820[a])	(11.54[c])
c/a	2.804	2.521	3.032	2.869
	(2.704[a])	(2.463[b])	(3.039[a])	(2.806[c])
$z_{P,As}$	0.6497	0.6379	0.6586	0.6537
	(0.6461[a])	(0.6366[b])	(0.6569[a])	(0.6524[c])
d(Ni-P(As))	2.264	2.393	2.261	2.370
	(2.264[a])		(2.260[a])	
[Ni-P(As)-Ni]	76.1	75.99	76.41	76.41

[a]Reference 21.
[b]Reference 18.
[c]Reference 19.

The hybridization effects were analyzed using the DOSs, which were obtained by a modified tetrahedron method.[24] The ionic bonding was considered using the Bader[25] analysis. In this approach, each atom of a crystal is surrounded by an effective surface that runs through minima of the charge density, and the total charge of an atom (the so-called Bader charge Q^B) is determined by integration within this region. In addition, some peculiarities of the intra-atomic bonding picture are visualized also by means of charge-density maps.

III. RESULTS AND DISCUSSION

A. Structural properties

As the first step, the total energy (E_{tot}) versus cell volume calculations were carried out to determine the equilibrium structural parameters for the considered ternary arsenides $(Sr,Ba)Ni_2(P,As)_2$. The calculated values are presented in Table I and are in reasonable agreement with the available experiments.[18,19,21] Some divergences are related to the well-known overestimation of the lattice parameters within local-density approximation (LDA)–GGA–based calculation methods.

At the same time, the results obtained allow us to make some interesting conclusions. As can be seen, when going from $SrNi_2P_2$ to $BaNi_2P_2$ and from $SrNi_2As_2$ to $BaNi_2As_2$, i.e., when Sr (atomic radius $R^{at}=2.15$ Å) is replaced by a larger Ba atom ($R^{at}=2.21$ Å), the interlayer distance grows appreciably (parameter c, by about 8–13%) and the param-

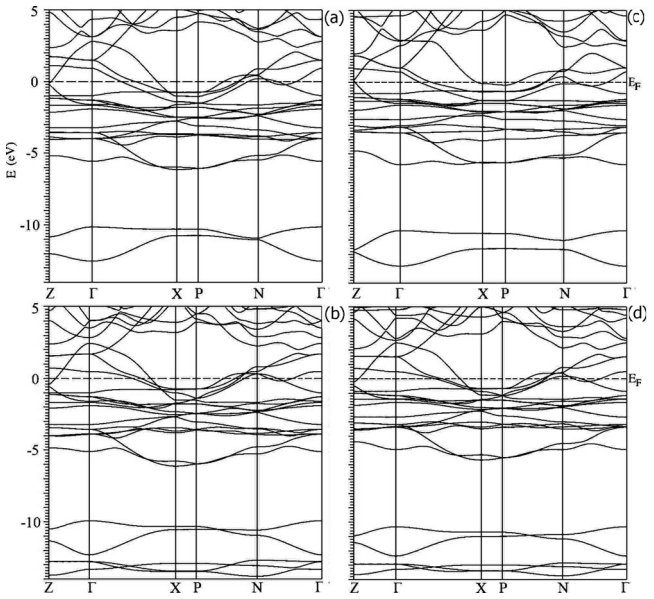

FIG. 2. Electronic band structures of (a) $SrNi_2P_2$, (b) $BaNi_2P_2$, (c) $SrNi_2As_2$, and (d) $BaNi_2As_2$.

eter a increases but slightly—by about 0.2–0.8%. This *anisotropic deformation* of the crystal structure is caused by strong *anisotropy of interatomic bonds*, i.e., by strong bonds inside [NiP(As)] layers versus relatively weak ionic coupling between adjacent [NiP(As)] layers and (Sr,Ba) atomic sheets; see below. On the other hand, when going from $SrNi_2P_2$ to $SrNi_2As_2$ and from $BaNi_2P_2$ to $BaNi_2As_2$, i.e., when a small P atom (R^{at}=1.30 Å) is replaced by a larger As atom (R^{at}=2.48 Å) inside [NiP(As)] layers, another type of anisotropic deformation takes place, namely, the parameter a grows with simultaneous compression of interlayer distances (lowering of the parameter c). This mechanism can be understood by taking into account the strengthening of As-As bonds (between adjacent [NiAs]/[NiAs] layers) versus P-P bonds (between adjacent [NiP]/[NiP] layers); see below. Note that similar anisotropic deformation of the crystal structure was reported for related tetragonal Bi-contained phases LaNiOBi and LaCuOBi.[26]

B. Electronic structure

Figures 2 and 3 show the band structures and total and atomic-resolved l-projected DOSs in ternary $(Sr,Ba)Ni_2(P,As)_2$ phases as calculated for equilibrium geometries, which are in reasonable agreement with available data for related Ni-based pnictides as obtained by means of FLAPW (Ref. 27) and tight-binding linear muffin-tin orbitals (TB-LMTO) (Ref. 28) calculations. In the band structure of $SrNi_2P_2$ the two lowest bands lying around −11 eV below the Fermi level (E_F) arise mainly from P 3s states and are separated from the near-Fermi valence bands by a gap. These bands are located in the energy range from −6.1 eV to E_F and are formed predominantly by P 3p and Ni 3d states. The corresponding DOSs include four subbands A, B, C, and D (Fig. 3); subbands A and B contain strongly hybridized Ni 3d–P 3p states which are responsible for the covalent

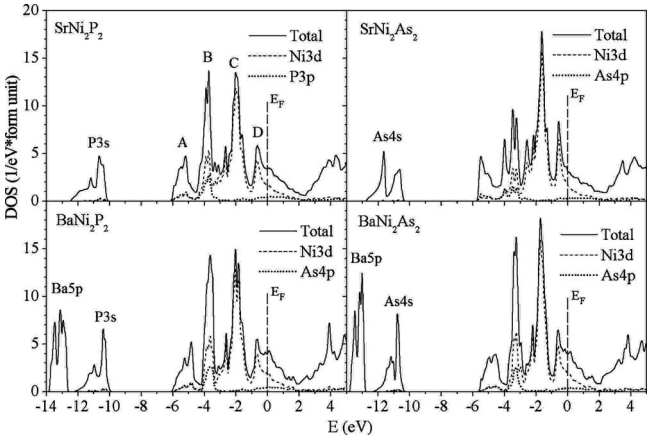

FIG. 3. Total and partial densities of states of $SrNi_2P_2$, $SrNi_2As_2$, $BaNi_2P_2$, and $BaNi_2As_2$.

Ni-P bonding. The intense peak C in the DOS is due to the Ni 3d–like bands with low $E(k)$ dispersion which are located around −2 eV and originate from quasi-two-dimensional Ni $3d_{xy}$ and Ni $3d_{x^2-y^2}$ electronic states. Finally, the topmost part of the valence band (subband D) is also made up basically of contributions from Ni 3d states with an admixture of antibonding P 3p states. These states participate in metallic-like Ni-Ni bonds. Thus, the DOS region near the Fermi level in $SrNi_2P_2$ is formed mainly by the states of [NiP] layers. Moreover, it is noteworthy that the contributions from the valence 5s states of Sr to the occupied subbands A–D are negligible, i.e., in $SrNi_2P_2$ these atoms are in the form of cations P^{2+}. This means that the Sr atomic sheets and the [NiP] layers are linked by ionic interactions; see also below.

Comparison of the band structures and DOS profiles of the isoelectronic and isostructural $SrNi_2P_2$, $BaNi_2P_2$, $SrNi_2As_2$, and $BaNi_2As_2$ shows that all these phases preserve the four-peak structure of the valence band, though the band dispersion $E(k)$ differs for phases with various types of pnictogen and alkaline-earth metal sublattices, i.e., it depends on their chemical composition and structural peculiarities (see above). These differences are seen from the data presented in Figs. 2 and 3 and Table II, where the band-structure parameters (the bandwidths) of $(Sr,Ba)Ni_2(P,As)_2$ phases are summarized. Another obvious difference is the width and composition of the quasicore states in the energy interval from −10 to −14 eV, where for Sr-containing phases only P(As) s states are located, while for Ba-containing phases the Ba 5p

TABLE II. Calculated values of bandwidths (in eV) for ternary pnictides $SrNi_2P_2$, $SrNi_2As_2$, $BaNi_2P_2$, and $BaNi_2As_2$.

System	$SrNi_2P_2$	$SrNi_2As_2$	$BaNi_2P_2$	$BaNi_2As_2$
Valence band	6.20	5.75	6.05	5.55
Band gap	3.95	4.88	3.89	4.80
Quasicore pnictogen s band	2.40	2.31	2.05	1.82
Band gap			0.30	0.52
Quasicore Ba 5p band			1.35	1.05

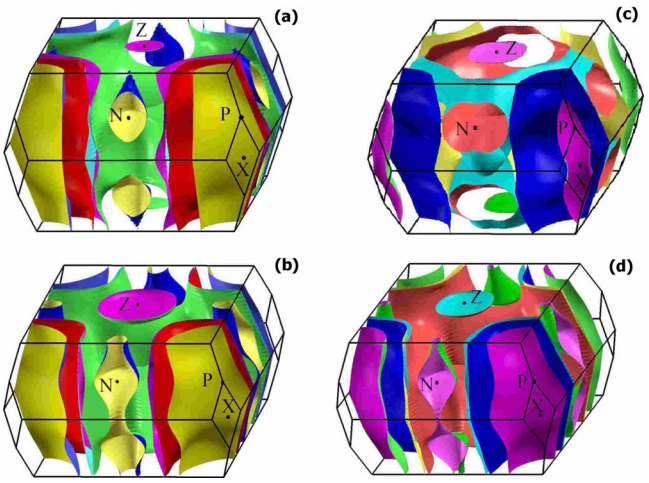

FIG. 4. (Color online) The Fermi surfaces of (a) $SrNi_2P_2$, (b) $BaNi_2P_2$, (c) $SrNi_2As_2$, and (d) $BaNi_2As_2$.

bands appear in the vicinity of these pnictogen-derived bands.

In turn, the above-mentioned common features of the band structure for the Ni-based phases reveal some important differences between these systems and AFe_2As_2—the parent phases for high-T_C 122 FeAs SCs. Really, in the AFe_2As_2 materials, the Fe ion has a nominal valence Fe^{2+} with six d electrons per Fe atom, whereas for $(Sr,Ba)Ni_2(P,As)_2$ phases the Ni ion has the same nominal valence Ni^{2+} but eight d electrons per Ni atom. For AFe_2As_2 phases, the Fermi level intersects the quasi-two-dimensional low-dispersive Fe $3d$–like bands which form the characteristic FS consisting of hole and electron cylindrical-like sheets along the k_z direction.[12,29] Owing to the growth of the electron concentration and the band filling for Ni-based phases, the Fermi level is shifted from a manifold of quasi-two-dimensional low-dispersive $3d$-like bands (subband C, Fig. 3) to the upper bands (subband D, Fig. 3) with higher dispersion $E(k)$, where large contributions from Ni d_{xz}, d_{yz}, and d_{z^2} orbitals, as well as from pnictogen p states, take place in addition to Ni d_{xy} and $d_{x^2-y^2}$ orbitals. As a result, the Fermi surfaces for $(Sr,Ba)Ni_2(P,As)_2$ phases differ markedly from the FSs of AFe_2As_2 phases and adopt a multisheet three-dimensional type; see Fig. 4.

As electrons near the Fermi surface are involved in the formation of the superconducting state, it is important to figure out their nature. The total and orbital decomposed partial DOSs at the Fermi level, $N(E_F)$, are shown in Table III. It is seen that for all Ni-containing phases the main contribution to $N(E_F)$ is from the Ni $3d$ states, which are responsible for the metallic properties of the materials. Let us note that the values of $N(E_F)$ for $(Sr,Ba)Ni_2(P,As)_2$ phases are lower than for related AFe_2As_2 materials [for example, for $BaNi_2As_2$ $N(E_F)=3.974$ $eV^{-1}/f.u.$ as compared with $N(E_F)=4.553$ $eV^{-1}/f.u.$ for $BaFe_2As_2$ (Ref. 13)], whereas the contributions of pnictogen p states to $N(E_F)$ in Ni-containing phases are higher [for example, for $BaNi_2As_2$ $N^{As}(E_F)/N^{Ni\,d}(E_F)=0.202$ as compared with $N^{As}(E_F)/N^{Fe\,d}(E_F)=0.038$ for $BaFe_2As_2$ (Ref. 13)]. According to our estimations, the values of the $N(E_F)$ of the Ni-containing materials decrease in the following sequence:

$$BaNi_2As_2 > BaNi_2P_2 > SrNi_2P_2 > SrNi_2As_2. \quad (1)$$

The obtained data also allow us to estimate the Sommerfeld constants (γ) and the Pauli paramagnetic susceptibility (χ) for ternary $(Sr,Ba)Ni_2(P,As)_2$ phases under the assumption of the free-electron model as $\gamma=(\pi^2/3)N(E_F)k_B^2$ and $\chi=\mu_B^2N(E_F)$. It is seen from Table III that both γ and χ decrease in sequence (1). On the other hand, the calculated γ values are lower than the available experimental data (Table III). It is no wonder, and it reflects the well-known fact of underestimation of the Sommerfeld constants in such calculations with neglecting of the electron-phonon interactions.[31]

The recent work by Shameem-Banu *et al.*[28] indicates that the superconducting properties of $BaNi_2As_2$ may be ex-

TABLE III. Total and partial densities of states at the Fermi level (in states/eV atom), electronic heat capacity γ (in mJ K^{-2} mol^{-1}), and molar Pauli paramagnetic susceptibility χ (in 10^{-4} emu/mol) for ternary pnictides $SrNi_2P_2$, $SrNi_2As_2$, $BaNi_2P_2$, and $BaNi_2As_2$. Available experimental data are given in parentheses.

System/parameter	Sr(Ba) $s+p$	P(As) s	P(As) p	P(As) d	Ni $4s$
$SrNi_2P_2$	0.021	0.030	0.411	0.023	0.024
$SrNi_2As_2$	0.013	0.037	0.274	0.012	0.029
$BaNi_2P_2$	0.034	0.028	0.448	0.028	0.027
$BaNi_2As_2$	0.030	0.025	0.350	0.013	0.024

System/parameter	Ni $4p$	Ni $3d$	Total	γ	χ
$SrNi_2P_2$	0.121	1.694	3.433	8.09	1.11
$SrNi_2As_2$	0.095	1.676	3.173	7.48 (8.7[a])	1.02
$BaNi_2P_2$	0.143	1.838	3.967	9.35	1.28
$BaNi_2As_2$	0.123	1.930	3.974	9.37 (11.6,[b] 12.3[c])	1.28

[a]Reference 18.
[b]Reference 19.
[c]Reference 30.

TABLE IV. Effective atomic charges and charges of [NiP(As)] layers (in e) for ternary pnictides $SrNi_2P_2$, $SrNi_2As_2$, $BaNi_2P_2$, and $BaNi_2As_2$ as obtained from a purely ionic model (Q^i), Bader analysis (Q^B), and their differences ($\Delta Q = Q^B - Q^i$).

System	Q	Ni	P(As)	[Sr(Ba)]	[NiP(As)]
$SrNi_2P_2$	Q^i	+2	−3	+2	−1
	Q^B	15.919	5.766	8.629	
	ΔQ	1.919	−2.234	0.629	−0.315
$SrNi_2As_2$	Q^i	14(+2)	8(−3)	8(+2)	−1
	Q^B	16.058	5.614	8.657	
	ΔQ	2.058	−2.386	0.657	−0.328
$BaNi_2P_2$	Q^i	14(+2)	5(−3)	10(+2)	−1
	Q^B	15.875	5.766	8.721	
	ΔQ	1.875	−2.234	0.721	−0.360
$BaNi_2As_2$	Q^i	14(+2)	8(−3)	8(+2)	−1
	Q^B	16.020	5.608	8.743	
	ΔQ	2.020	−2.392	0.743	−0.372

plained in terms of the conventional electron-phonon BCS theory. Therefore we used the calculated Sommerfeld constants γ^{theor} for simple estimations[32] of the average electron-phonon coupling constant λ as $\gamma^{\text{expt}} = \gamma^{\text{theor}}(1+\lambda)$. Within these crude estimations, using the available values of γ^{expt} for $SrNi_2As_2$ and $BaNi_2As_2$ (Refs. 18 and 19) and the calculated γ^{theor}, we obtained $\lambda \sim 0.16-0.24$ for these systems, i.e., these ternary pnictides are within the weak-coupling limit. For comparison, for other related 1111 and 122 phases, the available estimations of λ vary from 0.2 [for LaFeAsO (Ref. 33)] to 0.58 [for LaNiPO (Ref. 34)] and 0.76 [for $BaNi_2As_2$ (Ref. 27)].

One of the most intriguing peculiarities of FeAs SCs is the presence of typically metallic collective excitations, such as itinerant magnetization waves in the nonsuperconducting undoped parent 1111 or 122 phases such as LnFeAsO or AFe_2As_2 (Refs. 1–18) for which at least three different competing types of magnetic fluctuations have been predicted.[35–38] Within our band-structure calculations, the magnetic instability of ternary arsenides $(Sr,Ba)Ni_2(P,As)_2$ may be examined by the simple Stoner criterion, according to which magnetism may occur if $N(E_F)I > 1$. Here $N(E_F)$ is the density of states at the Fermi level on an atom per spin basis. Taking the typical value of $I = 0.9$,[39] our estimations show that the parameter $N(E_F)I$ changes from 0.71 (for $SrNi_2As_2$) to 0.89 (for $BaNi_2As_2$), which becomes most unstable to magnetism among all the considered ternary pnictides.

C. Chemical bonding

The conventional picture of the intra-atomic interactions in layers of 1111 and 122 phases assumes a strong intralayer bonding of a mixed type together with a relatively small ionic bonding between the adjacent molecular layers (atomic sheets). This strong bonding anisotropy determines the quasi-two-dimensional nature of these systems.[2,12,13,26,27,34,40] On the other hand, according to Yildirim,[38] in the AFe_2As_2 materials strong covalent As-As interactions occur both inside each [FeAs] layer and between adjacent [FeAs]/[FeAs] layers, and these strong interlayer As-As interactions lead to high isotropy of 122 systems.

Let us discuss the bonding in $(Sr,Ba)Ni_2(P,As)_2$ phases. To describe the *ionic bonding* for these materials, it is possible to start with a simple ionic picture, which considers the usual oxidation numbers of atoms: $(Sr,Ba)^{2+}$, Ni^{2+}, and $(P,As)^{3-}$. Thus, the charge states of the layers are $[Sr(Ba)]^{2+}$ and $\frac{1}{2}[NiP(As)]^{1-}$, i.e., the charge transfer occurs from $[Sr(Ba)]^{2+}$ sheets to $[NiP(As)]^{1-}$ layers. Furthermore, inside [NiP(As)] layers, the ionic bonding takes place between Ni-P(As) atoms.

To estimate the amount of electrons redistributed between the adjacent [Sr(Ba)] and [NiP(As)] layers and between the atoms inside each layer, we carried out a Bader[25] analysis, and the total charge of an atom (the so-called Bader charge Q^B) as well as the corresponding charges as obtained from the purely ionic model (Q^i) and their differences ($\Delta Q = Q^B - Q^i$) are presented in Table IV. These results show that the interlayer charge transfer is much smaller than it is predicted in the idealized ionic model. Namely, the transfer $\Delta Q([Sr(Ba)] \rightarrow [NiP(As)])$ is about $(0.32-0.37)e$; these values are smaller for Sr-containing phases than for their Ba-containing counterparts and are smaller for phosphides as compared with related arsenides. In addition, the "intralayer" transfer from Ni to pnictogen is higher for arsenides than for phosphides (Table IV).

The character of *covalent bonding* in $(Sr,Ba)Ni_2(P,As)_2$ phases may be well understood from site-projected DOS calculations. As shown in Fig. 3, Ni-P(As) states are strongly hybridized. These covalent bonds are clearly visible in Fig. 5, where the charge-density maps for $SrNi_2P_2$ and $SrNi_2As_2$ are depicted. In addition, the formation of covalent P(As)-P(As) bonds between adjacent [NiP(As)]/[NiP(As)] layers is clearly visible in Fig. 5, whereas no appreciable P(As)-P(As) bonds are present inside [NiP(As)] layers, in contrast to AFe_2As_2 materials.[38] In addition, it is seen in these charge-density maps that electron density between [NiAs]/[NiAs]

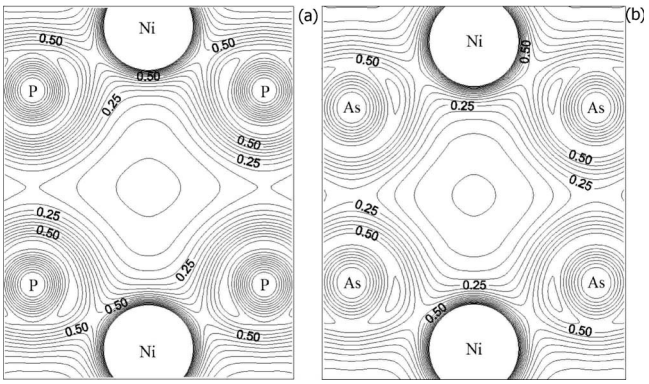

FIG. 5. Valence charge-density maps (in $e/\text{Å}^3$) in [100] plane for (a) $SrNi_2P_2$ and (b) $SrNi_2As_2$.

layers (i.e., along the As-As bond direction) is higher than along the P-P bond direction, which explains the above-mentioned contraction of the lattice parameter c in phosphides in comparison with arsenides.

Thus, summarizing the above results, the picture of chemical bonding for $(Sr,Ba)Ni_2(P,As)_2$ phases may be described in the following way:

(i) Inside [NiP(As)] layers, mixed covalent-ionic bonds Ni-P(As) take place (owing to hybridization of Ni 3d states and valence p states of pnictogen atoms and Ni→P(As) charge transfer).

(ii) Inside [NiP(As)] layers the metalliclike Fe-Fe bonds appear owing to delocalized near-Fermi Ni 3d states.

(iii) Between the adjacent [NiP(As)] layers and [Sr(Ba)] sheets, ionic bonds emerge owing to [NiP(As)]→[Sr(Ba)] charge transfer.

(iv) Between the adjacent [NiP(As)]/[NiP(As)] layers, covalent P(As)-P(As) bonds occur owing to hybridization of p-p states of pnictogen atoms.

(v) Generally, the bonding in $(Sr,Ba)Ni_2(P,As)_2$ phases can be classified as a high-anisotropic mixture of ionic, covalent, and metallic contributions.

IV. CONCLUSIONS

In summary, by means of the FLAPW-GGA approach, we have systematically studied the structural and electronic properties of the low-temperature superconductors tetragonal ternary Ni-based pnictides $SrNi_2As_2$, $BaNi_2As_2$, and $BaNi_2P_2$ in comparison with isostructural and isoelectronic $SrNi_2P_2$. Our results show that replacements of alkaline-earth metal (Sr↔Ba) and pnictogen (P↔As) type lead to anisotropic deformations of the crystal structure caused by strong anisotropy of interatomic bonds.

The electronic properties of all four Ni-based phases are very similar. This allows us to assume that $SrNi_2P_2$ may also exhibit low-temperature superconductivity. The near-Fermi valence bands in $(Sr,Ba)Ni_2(P,As)_2$ phases are derived basically from Ni 3d states with some admixture of antibonding P(As) p states.

As distinct from AFe_2As_2—the parent phases for 122 FeAs SCs—the Fermi level in $(Sr,Ba)Ni_2(P,As)_2$ phases is shifted from a manifold of quasi-two-dimensional low-dispersive 3d-like bands to the upper bands with higher dispersion $E(k)$ but lower DOS as a result of increased electron concentration. Therefore the Fermi surfaces for $(Sr,Ba)Ni_2(P,As)_2$ phases differ essentially from the FSs of AFe_2As_2 phases and adopt a multisheet three-dimensional type. Our estimations show also that $(Sr,Ba)Ni_2(P,As)_2$ are within the weak-coupling limit with a small average electron-phonon coupling constant $\lambda_{ep} \sim 0.16-0.24$.

Finally, our analysis reveals that bonding in $(Sr,Ba)Ni_2(P,As)_2$ is of a complex anisotropic character. Namely, the bonding in [NiP(As)] layers may be described as a mixture of metallic, ionic, and covalent contributions. In turn, between the adjacent [NiP(As)] layers and (Sr,Ba) atomic sheets, ionic bonds emerge, whereas between the adjacent [NiP(As)]/[NiP(As)] layers covalent bonds occur owing to hybridization of the p states of pnictogen atoms.

*Corresponding author; shein@ihim.uran.ru

[1] Y. Kamihara, T. Watanabe, M. Hirano, and H. Hosono, J. Am. Chem. Soc. **130**, 3296 (2008).
[2] D. Johrendt and R. Pottgen, Angew. Chem., Int. Ed. **47**, 4782 (2008).
[3] C. Wang, L. Li, S. Chi, Z. Zhu, Z. Ren, Y. Li, Y. Wang, X. Lin, Y. Luo, S. Jiang, X. Xu, G. Cao, and Z. Xu, EPL **83**, 67006 (2008).
[4] H. Takahashi, K. Igawa, K. Arii, Y. Kamihara, M. Hirano, and H. Hosono, Nature (London) **453**, 376 (2008).
[5] G. F. Chen, Z. Li, D. Wu, G. Li, W. Z. Hu, J. Dong, P. Zheng, J. L. Luo, and N. L. Wang, Phys. Rev. Lett. **100**, 247002 (2008).
[6] Z.-A. Ren, J. Yang, W. Lu, W. Yi, Z.-L. Shen, Z.-C. Li, G.-C. Che, X.-L. Dong, L.-L. Sun, F. Zhou, and Z.-X. Zhao, EPL **82**, 57002 (2008).
[7] X. H. Chen, T. Wu, G. Wu, R. H. Liu, H. Chen, and D. F. Fang, Nature (London) **453**, 761 (2008).
[8] M. Rotter, M. Tegel, D. Johrendt, I. Schellenberg, W. Hermes, and R. Pottgen, Phys. Rev. B **78**, 020503(R) (2008).
[9] M. Rotter, M. Tegel, and D. Johrendt, Phys. Rev. Lett. **101**, 107006 (2008).
[10] T. Park, E. Park, H. Lee, T. Klimczuk, E. D. Bauer, F. Ronning, and J. D. Thompson, J. Phys.: Condens. Matter **20**, 322204 (2008).
[11] P. M. Shirage, K. Miyazawa, H. Kito, H. Eisaki, and A. Iyo, Appl. Phys. Express **1**, 081702 (2008).
[12] D. J. Singh, Phys. Rev. B **78**, 094511 (2008).
[13] I. R. Shein and A. L. Ivanovskii, JETP Lett. **88**, 107 (2008).
[14] M. Tegel, D. Bichler, and D. Jorendt, Solid State Sci. **10**, 193 (2008).
[15] T. Watanabe, H. Yanagi, T. Kamiya, Y. Kamihara, H. Hiramatsu, M. Hirano, and H. Hosono, Inorg. Chem. **46**, 7719 (2007).
[16] I. R. Shein, V. L. Kozhevnikov, and A. L. Ivanovskii, Phys. Lett. A **372**, 5838 (2008).

[17] V. L. Kozhevnikov, O. N. Leonidova, A. L. Ivanovskii, I. R. Shein, B. N. Goshchitskii, and A. E. Kar'kin, JETP Lett. **87**, 649 (2008).
[18] E. D. Bauer, F. Ronning, B. L. Scott, and J. D. Thompson, Phys. Rev. B **78**, 172504 (2008).
[19] F. Ronning, N. Kurita, E. D. Bauer, B. L. Scott, T. Park, T. Klimczuk, R. Movshovich, and J. D. Thompson, J. Phys.: Condens. Matter **20**, 342203 (2008).
[20] T. Mine, H. Yanagi, T. Kamiya, Y. Kamihara, M. Hirano, and H. Hosono, Solid State Commun. **147**, 111 (2008).
[21] V. Keimes, D. Johrendt, A. Mewis, C. Hujnt, and W. Schlabitz, Z. Anorg. Allg. Chem. **623**, 1699 (1997).
[22] P. Blaha, K. Schwarz, G. K. H. Madsen, D. Kvasnicka, and J. Luitz, *WIEN2k, An Augmented Plane Wave Plus Local Orbitals Program for Calculating Crystal Properties* (Vienna University of Technology, Vienna, 2001).
[23] J. P. Perdew, K. Burke, and M. Ernzerhof, Phys. Rev. Lett. **77**, 3865 (1996).
[24] P. E. Blochl, O. Jepsen, and O. K. Andersen, Phys. Rev. B **49**, 16223 (1994).
[25] R. F. W. Bader, *Atoms in Molecules: A Quantum Theory*, International Series of Monographs on Chemistry (Clarendon, Oxford, 1990).
[26] I. R. Shein, V. L. Kozhevnikov, and A. L. Ivanovskii, Phys. Rev. B **78**, 104519 (2008).
[27] A. Subedi and D. J. Singh, Phys. Rev. B **78**, 132511 (2008).
[28] I. B. Shameem Banu, M. Rajagopalan, M. Yousuf, and P. Shenbagaraman, J. Alloys Compd. **288**, 88 (1999).
[29] S. E. Sebastian, J. Gillett, N. Harrison, P. H. C. Lau, D. J. Singh, C. H. Mielke, and G. G. Lonzarich, J. Phys.: Condens. Matter **20**, 422203 (2008).
[30] F. Ronning, N. Kurita, E. D. Bauer, B. L. Scott, T. Park, T. Klimczuk, R. Movshovich, and J. D. Thompson, J. Phys.: Condens. Matter **20**, 342203 (2008).
[31] W. L. McMillan, Phys. Rev. **167**, 331 (1968).
[32] Ch. Walti, E. Felder, C. Degen, G. Wigger, R. Monnier, B. Delley, and H. R. Ott, Phys. Rev. B **64**, 172515 (2001).
[33] L. Boeri, O. V. Dolgov, and A. A. Golubov, Phys. Rev. Lett. **101**, 026403 (2008).
[34] A. Subedi, D. J. Singh, and M. H. Du, Phys. Rev. B **78**, 060506(R) (2008).
[35] C. Krellner, N. Caroca-Canales, A. Jesche, H. Rosner, A. Ormeci, and C. Geibel, Phys. Rev. B **78**, 100504(R) (2008).
[36] S. Ishibashi, K. Terakura, and H. Hosono, J. Phys. Soc. Jpn. **77**, 053709 (2008).
[37] I. I. Mazin and M. D. Johannes, arXiv:0807.3737 (unpublished).
[38] T. Yildirim, arXiv:0807.3936 (unpublished).
[39] T. Beuerle, K. Hummler, C. Elsasser, and M. Fahnle, Phys. Rev. B **49**, 8802 (1994).
[40] I. R. Shein and A. L. Ivanovskii, Scr. Mater. **59**, 1099 (2008).